The Astrophysical Journal, 615:947–957, 2004 November 10

ATOMIC AND MOLECULAR EMISSION LINES FROM THE RED RECTANGLE[1]

L. M. Hobbs,[2] J. A. Thorburn,[2] T. Oka,[3] J. Barentine,[4] T. P. Snow,[5] and D. G. York[3]

Received 2004 May 27; accepted 2004 July 14

ABSTRACT

HD 44179 is the binary, post–asymptotic giant branch, central star of the Red Rectangle Nebula. Echelle spectra of the star have been obtained over a wavelength range from about 3800 to 10000 Å at a resolving power $R = 38,000$. A maximum S/N of 850 was achieved near 6800 Å. Fifty-seven identified atomic or ionic emission lines of 12 elements are detected in the star's spectrum, along with 76 emission lines of CH, CH^+, or CN. Three other CN lines are also present in absorption. Fewer than 30 of these 136 lines apparently have been previously reported, and the newly detected species include N II, Mg I, S II, K I, Fe I, Fe II, Rb I, Ba II, CH, and CN. On the basis of their shapes and widths, the line profiles of the various species can be classified into three groups: narrow, broad, or double-peaked. The emission apparently originates in an unusual, compact H II region and in associated neutral gas, both concentrated primarily within the small, dusty torus that optically obscures the central star. The detection of the Ba II emission from the gas may support the hypothesis of Waelkens et al. that HD 44179 is destined to become a barium star.

Subject headings: circumstellar matter — H II regions — stars: AGB and post-AGB — stars: evolution — stars: individual (HD 44179)

Online material: machine-readable tables

1. INTRODUCTION

The Red Rectangle is a biconical envelope that apparently was ejected recently by the post–asymptotic giant branch (post-AGB) star HD 44179. The nebula characteristically extends nearly 30″ or 20,000 AU from the star, while a much smaller (<0.″3), denser, roughly spherical volume with bipolar conical cavities appears to occupy the central region, out to about 100 AU (Men'shchikov et al. 2002; Cohen et al. 2004). The nebula displays a remarkable array of emission features in the UV, optical, infrared, and radio regions (Schmidt et al. 1980; Van Winckel et al. 2002). Many of the intensively studied but still unidentified features may originate primarily in relatively complex molecules that have formed within this unique envelope. Proposed candidates have included polycyclic aromatic hydrocarbons and some of the molecules that give rise to the unidentified diffuse interstellar bands seen in absorption toward reddened stars (Schmidt & Witt 1991; Scarrott et al. 1992). At $\lambda < 5000$ Å the dusty envelope becomes primarily, but not entirely, a reflection nebula (Vijh et al. 2004).

The spectrum of HD 44179 has also been investigated extensively. The star is a single-lined spectroscopic binary with a period of 318 days and $V = 8.8$ (Waelkens et al. 1996). High-resolution imaging shows that it is obscured by an optically opaque torus around the central region (Roddier et al. 1995; Bond et al. 1997), and the optical light received at the Earth from the star therefore arrives via scattering from dust that is located above and below the torus. Estimates of the star's properties deduced from its distance of about 700 pc and from an analysis of its spectrum via model stellar atmospheres include $L/L_\odot = 6000$, $T_{\rm eff} = 7700$ K, $\log g = 1.1$, and peculiar surface abundances characterized by strong deficiencies of many of the more refractory heavy elements (Waelkens et al. 1992). This composition is similar to that found in many cold, diffuse interstellar clouds. The star's present surface layers may therefore have been strongly contaminated by gas accreted, without the associated dust, from the surrounding torus and/or envelope, following previous ejection and cooling during the AGB phase (Van Winckel et al. 1995; Waelkens et al. 1996).

Relatively narrow emission lines seen in the stellar spectrum at the positions of the Hα, Na I D, and Ca II H and K lines further indicated the presence of an unusual H II region (Warren-Smith et al. 1981; Jura et al. 1997); at least one [O I] line was also detected (Van Winckel et al. 1995). A hot white dwarf, not yet unambiguously detected directly but presumably the originally more massive component of the binary, may provide the required ionizing photons (Men'shchikov et al. 2002). In our spectra of the star and of various positions in the envelope, the narrow emission lines appear brightest at the stellar position. Thus, the densest gas appears to be concentrated primarily within the conical cavities of the central region. Alternatively, at least some of the ground-level lines might arise from resonance scattering of the light from HD 44179, in which case the intensity of the emission lines generally declines with increasing distance of the scattering gas from the star. In addition, Waelkens et al. (1992), Balm & Jura (1992), Hall et al. (1992), and Bakker et al. (1997) discovered and identified 14 emission lines seen near 4230 Å in the spectrum of HD 44179 as members of the A–X(0–0) band of CH^+; some members of the (1–0) band were also detected (Van Winckel et al. 1995). These molecules appear to exist in a region of dense, cool neutral gas that adjoins the small, central volume of dense ionized gas. Furthermore, interferometric maps of the $J = 1$–0 and $J = 2$–1 emission from CO in a region extending to about 5″ around HD 44179 reveal that the CO-emitting gas exists in the form

[1] Based on observations obtained with the Apache Point Observatory 3.5 m telescope, which is owned and operated by the Astrophysical Research Consortium.

[2] University of Chicago, Department of Astronomy and Astrophysics, Yerkes Observatory, Williams Bay, WI 53191.

[3] University of Chicago, Department of Astronomy and Astrophysics, 5640 South Ellis Avenue, Chicago, IL 60037.

[4] Apache Point Observatory, P.O. Box 59, Sunspot, NM 88349-0059.

[5] University of Colorado, CASA-Campus Box 389, Boulder, CO 80309.

of an extended, orbiting disk (Glinski et al. 1997; Bujarrabal et al. 2003).

The primary purpose of this paper is to report the discovery of more than 100 additional, narrow, generally weaker emission lines that are present in the spectrum of HD 44179. Our nebular spectra, obtained at positions away from the central star, will be discussed separately in a future paper.

2. OBSERVATIONS

2.1. *The Spectra and Their Reduction*

The spectra of HD 44179 were obtained with the ARCES echelle spectrograph attached to the 3.5 m telescope at Apache Point Observatory (Wang et al. 2003). Information about similar ARCES spectra of other stars and about the data reduction methods also used here is provided by Thorburn et al. (2003); the present spectra were obtained as part of the larger program to observe the diffuse interstellar bands toward reddened stars at a signal-to-noise ratio (S/N) $\approx$ 1000. The results reported here are based on 12 individual exposures obtained on seven different nights between 2001 February 6 and 2004 February 3. The total exposure time accumulated was 5.7 hr. A log of the observations is presented in Table 1, where columns (2) and (3) respectively give the number of useful individual exposures acquired on each night and the corresponding total observing time. Each exposure provided nearly complete spectral coverage from about 3800 to 10000 Å at a resolving power of $R = 38,000$, or a velocity resolution of 8 km s^{-1} (FWHM). The resolution was measured directly from the widths of thorium comparison lines.

The rectangular entrance slit used measures $1\farcs6 \times 3\farcs2$ on the sky and cannot be rotated. Because the field observed at the Nasmyth focus rotates, the position angle of the slit varied with the hour angle at which the star was observed; in particular, for exposures of HD 44179 acquired on the meridian, the long axis of the slit was oriented northwest to southeast. Normal efforts were made both to center the star within the slit during each exposure and to center each exposure temporally near the meridian. However, in each of our spectra, in the direction transverse to the orders, there is no discernible spatial extension beyond the seeing disk of even the brighter emission lines described here. Thus, the fluxes received in these lines from points outside the seeing disk are very faint compared to that of the stellar continuum, and hence compared to the fluxes in the same lines from within the seeing disk, at each of the respective wavelengths. In brief, the rotation of the field introduced no apparent spatial averaging of the emission considered here.

The many telluric absorption lines of weak or intermediate strength that are present in the spectra have been largely removed through division of the spectra of HD 44179 by that of a telluric standard star; the details of the method will be described in a future paper. The method was of limited effectiveness for the very strong lines, however, and these reduced the precision with which a small number of blended emission lines from the Red Rectangle could be measured. Only a small subset of the many night-sky emission lines is bright enough to be seen above the stellar continuum, and no significant blending of such lines with those from the nebula was detected. The telluric emission lines were recognized by their invariant geocentric radial velocity and their spatial extension.

The heliocentric radial velocity of the star measured on each night is given in column (4) of Table 1, with a typical uncertainty of $\pm$0.4 km s^{-1}. The tabulated values are the respective averages of the velocities deduced from each of three representative stellar lines that show nearly symmetric, unblended profiles, suitably intermediate strengths, and accurately known laboratory wavelengths. The three lines are Fe II λ4923.927, C I λ4932.049, and C I λ5052.167. More importantly for our purposes, column (5) gives a weighted average heliocentric velocity for the K I λ7699 and [O I] λ6300 emission lines, referred to here succinctly as the velocity of "the gas." The K I line was given twice the weight of the [O I] line in forming the average, because the latter is weakly blended with a telluric line. The random errors again amount to about $\pm$0.4 km s^{-1} for these relatively strong emission lines (§ 2.2). In addition, the K I velocities are systematically more positive than those of O I by an offset, about 0.5 km s^{-1}, that is comparable to the random errors. The intrinsic widths of the two lines, about 15 and 25 km s^{-1}, respectively, are much larger than this offset. Furthermore, the two line widths are quite different from one another, and the offset probably results in part simply from this difference.

TABLE 1
LOG OF THE OBSERVATIONS

UT Date (1)	n (2)	t_{exp} (minutes) (3)	RV_{star}[a] (km s^{-1}) (4)	RV_{gas}[a,b] (km s^{-1}) (5)
2001 Feb 6	1	30	26.7	17.6
2002 Dec 30	2	60	17.7	19.5
2003 Nov 24	2	60	15.0	17.2
2004 Jan 3	1	10	12.4	19.7
2004 Jan 10	2	60	12.5	19.5
2004 Jan 31	2	60	10.9	19.4
2004 Feb 3	2	60	10.5	19.4

[a] To obtain LSR velocities, subtract 18.8 km s^{-1} from these heliocentric values.

[b] An average of the values obtained from the K I and O I emission lines, as described in § 2.1.

Within the uncertainties, the gas velocity was invariant on five of the seven nights in question, while a relative blueshift amounting to about one-fourth of a resolution element was observed on each of the other two nights, in 2001 and 2003. Therefore, we summed the whole set of exposures on a heliocentric velocity scale without attempting to register the emission lines further. The line profiles of all of the stronger emission lines, for which more precise data are available, showed generally modest amounts of temporal variability in shape, width, and equivalent width as well. The latter two parameters varied over full ranges of about 10% and 20%, respectively, in our data sets for the K I and the [O I] lines, for example. The widths and the equivalent widths of the line profiles reported below consequently are (properly weighted) averages over the seven nights in question. Little or no variability of any kind was observed over the four nights confined to a single month in 2004.

The summed stellar profiles, which are of minor interest here, will be smeared out by the variable stellar radial velocity. If the one night in 2001 is excluded from consideration, however, the intrinsic stellar line widths, about 38 km s^{-1} for typical weak lines, are much larger than all of the relative offsets among the various stellar velocities, so that this smearing will also be relatively minor.

After addition, these combined spectra yield an S/N of about 850 near 6800 Å, the wavelength at which the measured exposure level reaches a broad maximum. In nearby spectral regions that are free from adverse effects caused primarily by

interfering stellar or telluric lines or by cosmic-ray impacts on the CCD detector, the corresponding 3 σ detection limit amounts to an equivalent width $W_\lambda \approx 1.5$ mÅ, for a line (in either emission or absorption) with an intrinsic width of 15 km s^{-1}. The photometric precision falls monotonically to $S/N \approx 510$ at each of 4100 and 8800 Å. In the usual wavelength units, the corresponding detection limits are $W_\lambda \approx 1.5$ and 3.1 mÅ, respectively.

2.2. *Results*

Our final combined spectrum of HD 44179 shows at least 134 narrow, generally weak emission features, of which fewer than 30 (of H I, [O I], Na I, Ca II, or CH^+) have been previously reported in spectra obtained at lower resolution and S/N (Warren-Smith et al. 1981; Balm & Jura 1992; Van Winckel et al. 1995; Bakker et al. 1997). Data for 57 identified atomic or ionic emission lines of 12 elements are presented in Table 2. For each line, columns (3)–(8) respectively give the Einstein coefficient A; the product of the upper level statistical weight and the Einstein coefficient; the excitation potential, E/hc, of the upper level; the measured equivalent width; the intrinsic line width (FWHM), obtained by quadratic subtraction of the instrumental width from the measured line width; and the line-profile type, to be discussed in § 3.1. For lines consisting of two blended components, the width tabulated is the overall line width. In all but a few cases, the atomic data are taken from the online NIST compendium,[6] and the NIST multiplet numbers for the Fe I and [Fe II] multiplets are included in column (1). For emission lines with a common upper level, and for emission lines included within a given multiplet, the various equivalent widths should often be approximately proportional, in the optically thin limit, to the respective values of $g_{up}A$. Upper limits on some related (but undetected) lines are also presented in Table 2. In addition, the [N I] λ5200.26 line, not included in Table 2, is marginally seen in our data. The λ5197.90 line of the same multiplet is expected to be stronger by a factor near 2.6 but is blended with a stellar feature that precludes the needed confirmation.

For each line detected, the identification of the emitting species was made primarily on the basis of four familiar considerations. These are

1. the agreement between the observed and laboratory wavelengths, usually amounting to $\pm$0.02 Å or better, for at least two different lines of each atom, ion, or molecule, except Mg I and Rb I;
2. a satisfactorily low excitation potential for the upper level of the transition;
3. a general consistency between the observed and expected relative intensities of two or more lines of any given multiplet, when present, subject to the known observational errors in the line intensities and to possible errors in the adopted transition probabilities; and
4. a careful perusal of lists of other identified lines close to the wavelength in question, in both laboratory data and high-precision nebular observations in the literature.

Figure 1 shows the profiles of an illustrative subset of the observed lines. For comparison, the intrinsic width (FWHM) of a typical, weak stellar absorption line is 38 km s^{-1}. Also shown in Figure 1 and listed at the end of Table 2 is an unidentified emission line at 5105.57 Å ($\pm$0.02 Å), which shows a double-peaked profile similar to those of the Mg I], Fe I, Rb I, and Ba II lines. The observed wavelength coincides satisfactorily with that of a line of Cu I. If that identification were correct, a second Cu I line at 5782.13 Å arising from the same multiplet should also be detectable, but it is not seen with certainty. The relatively low cosmic abundance of Cu and the apparent absence of the companion line argue against an identification as Cu I.

Table 3 lists similar observational data for the molecular lines detected. These include three emission lines of CH that arise from the A–X (0–0) band (Fig. 2), 52 emission lines of CH^+ from six different bands of the A–X system (Fig. 3), and at least 21 weak emission lines of CN from the B–X (0–0) band (Fig. 4). Our spectra reveal measurable emission or absorption in neither the (1–0), (2–0), or (3–0) Phillips bands of C_2 (Thorburn et al. 2003) nor the 4051.6 Å band of C_3 (Oka et al. 2003). The laboratory wavelengths adopted in Table 3 are taken from Zachwieja (1995), Carrington & Ramsay (1982), and Prasad et al. (1992) for CH, CH^+, and CN, respectively. For CH, the values of the Einstein coefficient A are those of Luque & Crosley (1996). For CH^+ and CN, the values were calculated from the oscillator strengths given by Larsson & Siegbahn (1983) and Bauschlicher et al. (1988), respectively. In contrast to all of the other lines reported here, the $R(0)$, $R(1)$, and $P(1)$ lines of CN are seen in absorption; they will be considered further in § 3.2. Most of the CN lines are only marginally stronger than our detection limit in the near-UV region, and the widths (and the radial velocities) of these lines generally cannot be measured as accurately as those of the other lines in Tables 2 and 3. Therefore, the average of the widths of six relatively strong, well-defined emission lines has been adopted in Table 3 for each of those lines.

More generally, the errors in measuring both the radial velocities and the widths of most of the weaker emission lines in Tables 2 and 3 range up to 2 km s^{-1}, while profile asymmetries, blends with telluric, stellar, or other emission lines, or cosmic-ray impacts on the CCD detector correspondingly increase the uncertainties. Within these respective uncertainties, all of the lines in Tables 2 and 3 show a radial velocity that agrees with the average value for K I and O I given in Table 1, on each of the seven nights. The more intense CO emission reported by Bujarrabal et al. (2003) is also largely confined to heliocentric velocities 17 km $s^{-1} \leq RV \leq 20$ km s^{-1}.

3. COMMENTS

3.1. *Atomic Lines*

In H II regions and planetary nebulae, the forbidden lines of [C I], [O I], and Mg I], as well as the resonance lines of Na I, K I, and Ca II (H and K), originate either in neutral density condensations (Dinerstein et al. 1995) or in the transition regions from ionized to neutral hydrogen (Osterbrock 1989). All of these lines arise from species with ionization potentials below (or, for O I, effectively equal to) that of H I. The [N II] and the [S II] lines are strong in H II regions (Baldwin et al. 2000) and in low-ionization planetary nebulae (Sharpee et al. 2003), and H I lines are seen universally. The other lines reported in Table 2 are more seldom seen, especially the various permitted lines that arise mostly from radiative recombination, not electron excitation or resonance fluorescence. In particular, we are unaware of any previous detections of the Rb I or Ba II lines from H II regions, planetary nebulae, or circumstellar envelopes, except probably for some of the Ba II lines in the case of the planetary nebula NGC 7027 (Pequignot & Baluteau 1994).

[6] See http://physics.nist.gov/cgi-bin/AtData/main_asd.

TABLE 2

ATOMIC EMISSION LINES

Atom (1)	λ (Å) (2)	A (s^{-1}) (3)	$g_{up}A$ (s^{-1}) (4)	E_{up}/hc (cm^{-1}) (5)	W_λ (mÅ) (6)	FWHM (km s^{-1}) (7)	Profile Class[a] (8)
H I	6562.81	...	7.9(+8)	97,492	>1350	>18	2
	4861.34	...	2.7(+8)	102,824	>49	>11	2
[C I]	9850.26	1.8(−4)	9.0(−4)	10,193	10.5	7.5	1
	9824.13	6.1(−5)	3.0(−4)	10,193	<7	...	1
	8727.13	6.3(−1)	6.3(−1)	21,648	21	8.5	1
	4621.57	2.1(−3)	2.1(−3)	21,648	<2	...	1
[N II]	6583.45	2.7(−3)	1.4(−2)	15,316	22	40	2
	6548.05	9.2(−4)	4.6(−3)	15,316	4.5	39	2
	5754.59	1.2(+0)	1.2(+0)	32,689	<4	...	2
[O I]	6363.78	1.8(−3)	9.1(−3)	15,868	31	25	2
	6300.30	5.7(−3)	2.9(−2)	15,868	90	26	2
	5577.34	1.3(+0)	1.3(+0)	33,793	<8	...	2
Na I	5895.92	6.2(+7)	1.2(+8)	16,956	>540	19	3
	5889.95	6.2(+7)	2.5(+8)	16,973	>556	19	3
Mg I]	4571.10	4.3(+2)	1.3(+3)	21,870	9.5	27	3
[S II]	6730.82	8.8(−4)	3.5(−3)	14,853	17.5	23	2
	6716.44	2.6(−4)	1.6(−3)	14,885	7.5	23	2
	4076.35	1.3(−1)	2.7(−1)	24,525	<2	...	2
	4068.60	3.4(−1)	1.4(+0)	24,572	3.5	15	2
K I	7698.97	3.8(+7)	7.6(+7)	12,985	99	15	1
	7664.91	3.9(+7)	1.5(+8)	13,043	110	14	1
Ca II	8662.14	1.1(+7)	2.2(+7)	25,192	p[b]	...	1
	8542.09	9.8(+6)	3.9(+7)	25,414	30:	11:	1
	8498.02	1.1(+6)	4.4(+6)	25,414	...	...	1
	3968.47	1.4(+8)	2.8(+8)	25,192	>402	12	1
	3933.66	1.5(+8)	5.9(+8)	25,414	>340	12	1
[Ca II]	7323.89	1.3(+0)	5.2(+0)	13,650	58	11	1
	7291.47	1.3(+0)	7.8(+0)	13,711	88	11	1
Fe I (1)	5225.53	1.3(+3)	4.0(+3)	20,020	<5	...	3
	5204.58	2.3(+3)	1.1(+4)	19,912	5	26	3
	5168.90	3.8(+3)	2.7(+4)	19,757	<15	...	3
	5166.28	1.5(+3)	1.6(+4)	19,351	<4	...	3
	5110.41	4.9(+3)	4.4(+4)	19,562	5.5	26	3
Fe I (2)	4489.74	1.2(+4)	3.6(+4)	23,245	4	26	3
	4482.17	2.1(+4)	1.1(+5)	23,192	6.5	23	3
	4461.65	3.0(+4)	2.1(+5)	23,111	6.5	26	3
	4435.15	4.7(+3)	1.4(+4)	23,245	<3	...	3
	4427.31	3.4(+4)	3.1(+5)	22,997	5.5	29	3
	4375.93	3.0(+4)	3.2(+5)	22,846	3	25	3
Fe I (3)	4291.47	...	...	23,711	3.5	27	3
	4258.32	2.5(+3)	1.8(+4)	24,181	5.5	22	3
	4216.18	1.8(+4)	1.7(+5)	23,711	3.0	24	3
	4206.70	7.2(+3)	5.0(+4)	24,181	3.5	25	3
	4199.97	...	...	24,507	<2.5	...	3
Fe I (35)	5506.78	5.0(+4)	3.5(+5)	26,140	<5	...	3
	5497.52	6.3(+4)	3.1(+5)	26,340	2.5	26	3
	5455.61	...	...	26,479	13	28	3
	5446.92	5.3(+5)	2.7(+6)	26,340	14	28.5	3
	5434.52	1.7(+6)	1.7(+6)	26,550	11.5	27.5	3
	5429.70	4.3(+5)	3.0(+6)	26,140	12	28	3
	5405.77	1.1(+6)	3.3(+6)	26,479	21	30	3
	5397.13	2.6(+5)	2.3(+6)	25,900	8.5	27.5	3
	5371.49	1.1(+6)	5.3(+6)	26,340	24	28	3
	5328.04	1.2(+6)	8.1(+6)	26,140	25	27	3
	5269.54	1.3(+6)	1.1(+7)	25,900	33	27	3
Fe I (36)	5151.91	2.4(+4)	1.2(+5)	27,560	<2	...	3
	5150.84	3.1(+4)	2.2(+5)	27,395	2.5	32	3
	5123.72	7.2(+4)	2.2(+5)	27,666	5.5	25	3
	5107.45	4.2(+4)	2.1(+5)	27,560	3	28	3
	5083.34	4.1(+4)	2.8(+5)	27,395	5.5	30	3
	5079.74	5.2(+4)	1.6(+5)	27,666	3.5	33	3
	5051.63	4.7(+4)	4.2(+5)	27,167	<30	...	3
	5012.07	5.5(+4)	6.1(+5)	26,875	<5	...	3

TABLE 2—*Continued*

Atom (1)	λ (Å) (2)	A (s^{-1}) (3)	$g_{up}A$ (s^{-1}) (4)	E_{up}/hc (cm^{-1}) (5)	W_λ (mÅ) (6)	FWHM (km s^{-1}) (7)	Profile Class[a] (8)
	4994.13	3.2(+4)	2.2(+5)	27,395	2.5	26	3
[Fe II] (7).....	4452.10	5.2(−1)	3.1(+0)	23,318	<3	...	1
	4413.78	8.1(−1)	4.9(+0)	23,318	<2.5	...	1
	4359.33	1.1(+0)	6.6(+0)	23,318	3	14	1
	4287.39	1.5(+0)	9.0(+0)	23,318	5	17	1
[Fe II] (14).....	5376.45	2.6(−1)	2.1(+0)	21,712	<2	...	1
	5333.65	2.6(−1)	2.6(+0)	21,582	<3	...	1
	5261.62	3.1(−1)	3.7(+0)	21,430	<2	...	1
	5158.78	4.4(−1)	6.2(+0)	21,252	2.5	15	1
[Fe II] (15).....	5020.23	1.8(−1)	7.2(−1)	23,031	<2.5[c]	...	1
	4905.34	2.2(−1)	1.8(+0)	22,810	<2	...	1
	4814.53	4.0(−1)	4.0(+0)	22,637	5[d]	14	1
Rb I.....	7947.60	3.6(+7)	7.2(+7)	12,579	<8	...	3
	7800.27	3.8(+7)	1.5(+8)	12,817	7	22	3
Ba II.....	6496.90	3.3(+7)	6.6(+7)	20,262	7	29	3
	6141.72	3.7(+7)	1.5(+8)	21,952	9	30	3
	5853.68	4.8(+6)	1.9(+7)	21,952	<3	...	3
	4934.08	9.5(+7)	1.9(+8)	20,262	11	32	3
	4554.03	1.2(+8)	4.7(+8)	21,952	9	32	3
UID	5105.57	...	...	...	9.5	31	3

NOTE.—Table 2 is also available in machine-readable form in the electronic edition of the *Astrophysical Journal*.
[a] 1 = narrow, 2 = broad, 3 = double-peaked (or flat-topped); see § 3.1.
[b] Present, but severely obscured by the stellar Ca II line.
[c] Blended with the stronger CH^+ (1–2) $R(1)$ line.
[d] Includes the weaker CH^+ (0–1) $P(3)$ line.

Detections of other *s*-process elements in emission in higher ionization states in high-excitation planetary nebulae are becoming more common (Sterling & Dinerstein 2003).

On the basis of their shapes and widths observed at our instrumental resolution of 8 km s^{-1}, the line profiles of the various elements can be classified into three groups: narrow, broad, and double-peaked (or flat-topped). (An exception is the [N I] λ5200.26 line noted in § 2.2, which, if real, is too weak to permit such classification.) Each of the lines of [C I], K I, Ca II, [Ca II], and [Fe II] consists primarily of a relatively narrow, roughly symmetric, apparently single component with an intrinsic width generally not exceeding 15 km s^{-1}. These conclusions also apply to the lines of CH, CH^+, and CN. All of these narrow-lined species may therefore exist together in largely neutral gas in which the molecules survive. The two members of the K I and the Ca II doublets (and of the Na I doublet) respectively show roughly equal intensities; the gas in which the emission is produced appears to show appreciable optical depths to these lines.

The lines of [O I], [S II], and especially [N II] are generally broader. Like the narrower lines, they do not reveal the obvious presence of multiple, blended components that materially increase the overall line widths. The Hα line shows a complex structure, including a very broad component (Jura et al. 1997). All four of these broad-lined species presumably exist within the ionized gas.

Along with the unidentified line, the lines of Mg I], Fe I, Rb I, and Ba II are also relatively broad. However, all of the profiles of these generally very weak lines can be decomposed satisfactorily, if not uniquely, into two narrower, blended components of Gaussian shape. Each would then consist of two components of comparable strength that are split by roughly 14 km s^{-1}. The velocity centroids of the blends coincide, within the uncertainties, with those of the narrow, unblended lines of [C I], K I, and others noted above. If the lines are decomposed into two lines specifically of equal width, this width proves to be about 12 km s^{-1}, similar to those of the narrow, unblended lines. The Na I emission lines can also be construed to be of a similar form, except that the component near +25 km s^{-1} is appreciably weaker than the component near +13 km s^{-1}. The spatial location of all six of these species whose profiles may consist of two narrower, blended components is unclear, although the line widths inferred seem to favor the neutral gas. The double-peaked profiles may suggest an origin in a rotating disk of gas, a conclusion similarly reached for the CO molecules (Bujarrabal et al. 2003).

In *Hubble Space Telescope* (*HST*) spectra with an instrumental resolution FWHM > 25 km s^{-1}, Glinski et al. (1997) measured and analyzed the permitted λ1931 line of C I, whose upper and lower levels show excitation potentials $E/hc =$ 61,982 and 10,193 cm^{-1}, respectively. The observed line consists of a very broad absorption feature, to which blended stellar lines may contribute weakly, plus a much narrower emission feature. The latter shows a width and a radial velocity that are roughly consistent with those of most of the emission lines observed here. However, the velocity resolution of the *HST* spectra is inadequate to distinguish to which of our three line groups the emission component of the λ1931 line may belong. In particular, no conclusive comparison of the emission feature's intrinsic width is possible with those of the two narrow, forbidden [C I] lines listed in Table 2.

The detection of the four Ba II emission lines is particularly striking. No photospheric Ba II absorption lines are seen in our spectra, although such lines are detected in the spectra of some other metal-poor supergiants (Smith & Lambert 1987; Waelkens et al. 1991). Perhaps the barium now located in the circumstellar gas was produced via the *s*-process within the

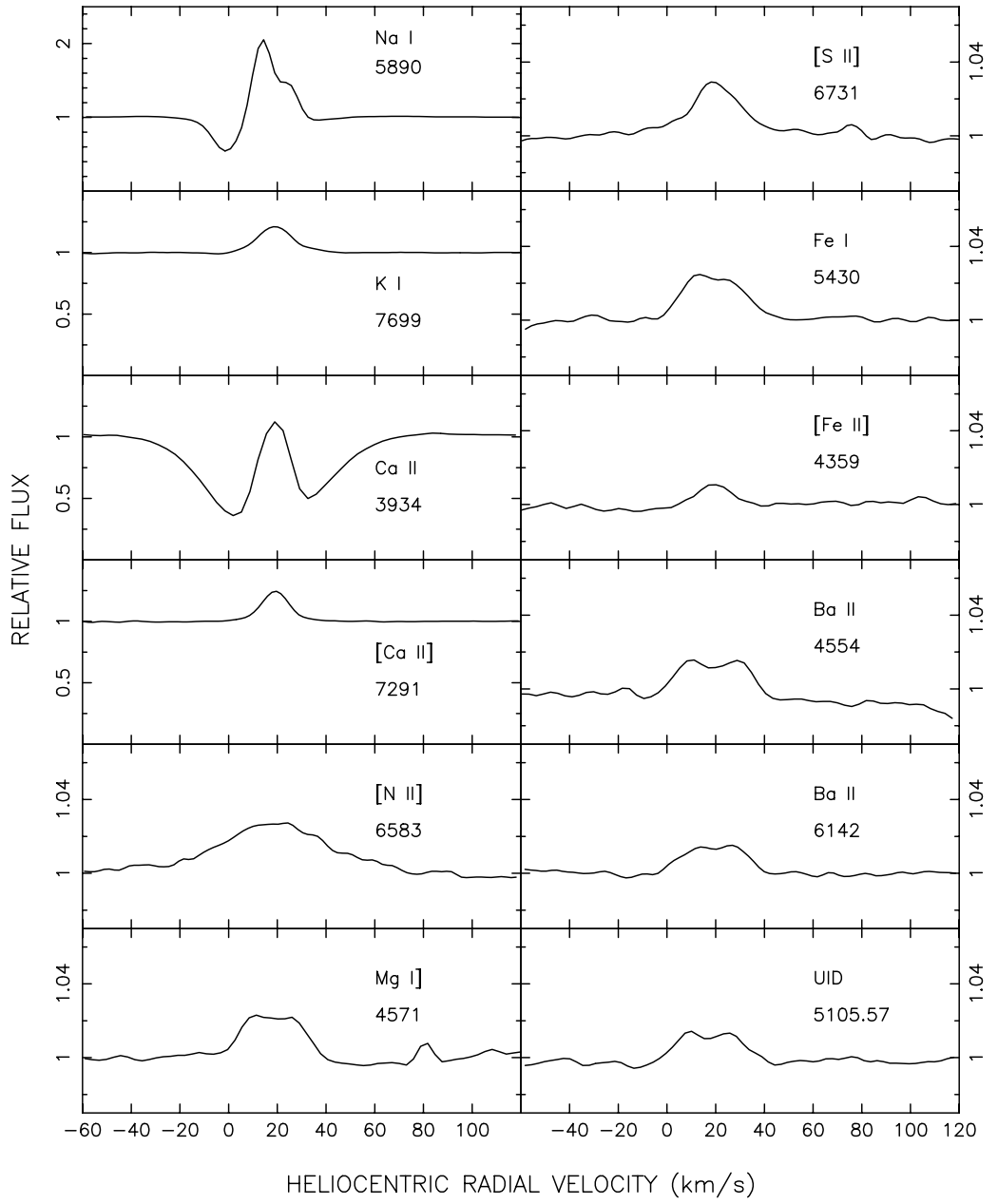

FIG. 1.—Profiles of 12 atomic or ionic emission lines in the spectrum of HD 44179. The instrumental broadening corresponds to 8 km s^{-1}, and the local stellar continuum has been set to unit flux in each panel. Note the differences among the vertical scales for the various panels, as well as the presence of the stellar absorption lines of Na I and Ca II. The strongest of the emission lines shown is the Na I D2 line (Table 2). The somewhat weaker lines of K I, Ca II, and [Ca II] are shown at an expanded, common scale, while seven much weaker lines of five other elements are plotted to a further expanded, common scale. The unidentified line at 5105.57 Å is also shown with the latter group, on an approximate velocity scale. The additional, very narrow, weak feature apparently adjacent to the Mg I] line arises from noise and is not real. Any telluric absorption lines present have been removed through division of the star's spectrum by that of a telluric standard star.

proposed white dwarf companion, while that star was previously on the AGB. If some of the barium was eventually ejected along with the star's surface layers, some of the ejected material could now be in transit to the currently luminous, post-AGB star, whose surface abundances seem to reveal the action of a peculiar accretion process (§ 1). Despite its already advanced evolutionary state, the post-AGB star may yet be destined to become a barium star, as Waelkens et al. (1996) have suggested on independent grounds.

3.2. *Molecular Lines*

No detections of either CH or CN in the spectrum of HD 44179 seem to have been reported previously; in addition, our list greatly expands on the 14 relatively strong CH^+ lines already known (Bakker et al. 1997). To the best of our knowledge, HD 44179 is the only object other than comets from which the optical spectra of CH, CH^+, and CN are observed in emission. A number of far-infrared rotational emission lines of CH^+, from levels up to $J = 6$, have been detected from the photodissociation region surrounding the planetary nebula NGC 7027 (Cernicharo et al. 1997). Often precursors to planetary nebulae, the envelopes around some AGB and post-AGB stars contain an extensive set of polyatomic molecules (Cernicharo 2004).

From the observed relative intensities of the lines of the CH^+ (0–0) band, a rotational temperature near 200 K has been

TABLE 3
MOLECULAR EMISSION LINES

Molecule	Band	Line	λ (Å)	$10^{-5} \times A$ (s^{-1})	E_{up}/hc (cm^{-1})	W_λ (mÅ)	FWHM (km s^{-1})
CH.....	A–X	$R_2(5/2)$	4291.16	7.2	23,464.87	<2	...
	(0–0)	$R_1(7/2)$	4292.08	7.3	23,464.05	<2	...
	...	$R_2(3/2)$	4296.62	7.6	23,348.84	<2	...
	...	$R_1(5/2)$	4297.99	8.0	23,347.69	2.5	13
	...	$R_2(1/2)$	4300.31	9.3	23,261.92	3	11
	...	$R_1(3/2)$	4303.93	9.2	23,260.16	4.5	11
	...	...	...	...	...	...	...
CH+.....	A–X	$R(2)$	3954.37	8.1	25,364.83	14.5[a]	11
	(1–0)	$R(3)$	3954.37	7.9	25,448.27	...	...
	...	$R(1)$	3955.49	8.5	25,302.04	14[b]	11
	...	$R(4)$	3955.49	7.8	25,552.25	...	...
	...	$R(0)$	3957.69	9.5	25,260.11	11[c]	11
	...	$R(5)$	3957.75	7.6	25,676.44	...	...
	...	$R(6)$	3961.17	7.6	25,820.58	<4	...
	...	$Q(1)$	3962.07	14.1	25,260.04	13.5	10
	...	$Q(2)$	3964.25	14.1	25,301.83	14.5	10.5
	...	$Q(3)$	3967.54	14.1	25,364.39	10	10.5
	...	$P(2)$	3970.82	4.7	25,260.11	<18	...
	...	$Q(4)$	3971.94	14.0	25,447.57	<12	...
	...	$P(3)$	3977.38	5.6	25,302.04	8.5	10
	...	$Q(5)$	3977.47	14.0	25,551.18	<4	...
	...	$Q(6)$	3984.16	13.9	25,674.97	<2.5	...
	...	$P(4)$	3985.04	6.0	25,364.81	5	9
	...	$P(5)$	3993.82	6.1	25,448.28	4	10.5
	...	$P(6)$	4003.74	6.2	25,552.24	3	11
	...	$P(7)$	4014.83	6.3	25,676.43	2.5	12
	...	...	...	...	...	...	...
	(2–1)	$R(2)$	4171.16	5.4	26,787.66	<2	...
	...	$R(1)$	4171.74	5.7	26,730.58	2.5	9
	...	$R(3)$	4171.96	5.3	26,863.52	<2	...
	...	$R(0)$	4173.70	6.3	26,692.45	<5	...
	...	$Q(1)$	4178.40	9.4	26,692.39	<8	...
	...	$Q(2)$	4181.15	9.4	26,730.39	2	9
	...	$Q(3)$	4185.28	9.4	26,787.27	2.5	8
	...	$P(2)$	4187.79	3.1	26,692.45	<2	...
	...	$Q(4)$	4190.82	9.3	26,862.87	2	10
	...	$P(3)$	4195.24	3.7	26,730.58	<2	...
	...	$Q(5)$	4197.79	9.3	26,957.00	<2	...
	...	...	...	...	...	...	...
	(0–0)	$R(4)$	4225.27	11.2	23,938.51	6	9.5
	...	$R(3)$	4225.70	11.4	23,825.04	13	11.5
	...	$R(5)$	4225.80	11.0	24,074.16	<4	...
	...	$R(2)$	4227.06	11.7	23,733.98	14	10
	...	$R(6)$	4227.31	10.9	24,231.68	<2	...
	...	$R(1)$	4229.35	12.3	23,665.51	23	11
	...	$R(0)$	4232.55	13.6	23,619.78	18	10.5
	...	$Q(1)$	4237.56	20.3	23,619.70	31	10.5
	...	$Q(2)$	4239.38	20.3	23,665.26	29.5	10.5
	...	$Q(3)$	4242.11	20.3	23,733.49	21	10
	...	$Q(4)$	4245.78	20.2	23,824.25	15	11.5
	...	$P(2)$	4247.57	6.7	23,619.78	9.5	11
	...	$Q(5)$	4250.38	20.2	23,937.35	7.5	10
	...	$P(3)$	4254.39	8.0	23,665.51	13.5	9.5
	...	$Q(6)$	4255.95	20.1	24,072.54	4	12.5
	...	$P(4)$	4262.12	8.6	23,733.97	12	9.5
	...	$Q(7)$	4262.52	20.0	24,229.53	2	11
	...	$Q(8)$	4270.09	19.9	24,408.01	<2	...
	...	$P(5)$	4270.78	8.8	23,825.04	6	11
	...	$P(6)$	4280.38	9.0	23,938.49	6.5	12
	...	$P(7)$	4290.94	9.0	24,074.15	<3	...
	...	...	...	...	...	...	...
	(1–1)	$R(1)$	4436.19	1.8	25,302.04	1.5	9
	...	$R(0)$	4439.16	2.0	25,260.11	<1.5	...
	...	$Q(1)$	4444.48	3.0	25,260.04	2.5	10
	...	$Q(2)$	4446.84	3.0	25,301.83	2	10
	...	$Q(3)$	4450.39	3.0	25,364.39	<2	...
	...	$P(2)$	4455.11	1.0	25,260.11	2[d]	9
	...	$Q(4)$	4455.15	3.0	25,447.57	...	...

TABLE 3—*Continued*

Molecule	Band	Line	λ (Å)	$10^{-5} \times A$ (s^{-1})	E_{up}/hc (cm^{-1})	W_λ (mÅ)	FWHM (km s^{-1})
	...	*P*(3)	4462.97	1.2	25,302.04	<3	...
	...	...	...	...	...	...	...
	(0–1)	*R*(3)	4777.80	1.8	23,825.04	1.5	9
	...	*R*(2)	4780.22	1.8	23,733.98	4	11
	...	*R*(1)	4783.59	1.9	23,665.51	3	9.5
	...	*R*(0)	4787.91	2.0	23,619.78	3	9.5
	...	*Q*(1)	4794.10	3.1	23,619.71	5	9
	...	*Q*(2)	4795.97	3.1	23,665.26	5	9.5
	...	*Q*(3)	4798.80	3.1	23,733.49	4.5	9.5
	...	*Q*(4)	4802.58	3.1	23,824.25	4	9
	...	*P*(2)	4806.46	1.0	23,619.78	1.5	10.5
	...	*Q*(5)	4807.35	3.1	23,937.35	2.5	12
	...	*Q*(6)	4813.12	3.1	24,072.54	<3	...
	...	*P*(3)	4814.51	1.2	23,605.51	<5[e]	...
	...	*Q*(7)	4819.93	3.1	24,229.53	<2	...
	...	*P*(4)	4823.50	1.3	23,733.97	2	11.5
	...	*P*(5)	4833.45	1.4	23,825.04	<1.5	...
	...	...	...	...	...	...	...
	(1–2)	*R*(2)	5017.57	1.5	25,364.83	<6	...
	...	*R*(1)	5020.33	1.6	25,302.04	2.5[f]	9
	...	*R*(0)	5024.38	1.8	25,260.11	4.5	11
	...	*Q*(1)	5030.95	2.6	25,260.04	3	12
	...	*Q*(2)	5033.48	2.6	25,301.83	3	11
	...	*Q*(3)	5037.29	2.6	25,364.39	1.5	11.5
	...	*P*(2)	5044.07	0.9	25,260.11	<2	...
	...	*P*(3)	5053.17	1.0	25,302.04	<4	...
	...	...	...	...	...	...	...
CN.....	*B*–*X*	*R*(15)	3863.39	7.2	26,330.16	<1.5	...
	(0–0)	*R*(14)	3864.30	7.2	26,267.44	2.3	...
	...	*R*(13)	3865.15	7.2	26,208.88	2.7	...
	...	*R*(12)	3865.99	7.1	26,154.13	2.2	...
	...	*R*(11)	3866.82	7.1	26,103.26	2.8	13[g]
	...	*R*(10)	3867.63	7.1	26,056.30	3.4	13[g]
	...	*R*(9)	3868.41	7.1	26,013.25	3.7	13[g]
	...	*R*(8)	3869.18	7.0	25,974.10	2.7	13[g]
	...	*R*(7)	3869.93	7.0	25,938.87	3.3	13[g]
	...	*R*(6)	3870.67	6.9	25,907.47	2.9	...
	...	*R*(5)	3871.37	6.8	25,880.11	2.3	...
	...	*R*(4)	3872.05	6.7	25,856.62	2.4	...
	...	*R*(3)	3872.72	6.6	25,837.06	<1.5	...
	...	*R*(2)	3873.37	6.4	25,821.36	<1.5	...
	...	*R*(1)	3874.00	5.9	25,809.62	2.5[h]	<6
	...	*R*(0)	3874.61	4.9	25,801.79	3.5[h]	<6
	...	*P*(1)	3875.76	14.8	25,797.87	2.7[h]	<6
	...	*P*(2)	3876.31	9.9	25,801.79	<1.5	...
	...	*P*(3)	3876.84	8.9	25,809.62	1.5	...
	...	*P*(4)	3877.35	8.5	25,821.37	3.5	13[g]
	...	*P*(5)	3877.83	8.2	25,837.06	1.6	...
	...	*P*(6)	3878.30	8.1	25,856.62	1.5	...
	...	*P*(7)	3878.75	8.0	25,880.12	2.1	...
	...	*P*(8)	3879.18	7.9	25,907.47	3.1	...
	...	*P*(9)	3879.58	7.8	25,938.87	3.4	...
	...	*P*(10)	3879.96	7.8	25,974.10	2.6	...
	...	*P*(11)	3880.33	7.8	26,013.25	1.9	...
	...	*P*(12)	3880.67	7.7	26,056.30	2.2	...

NOTE.—Table 3 is also available in machine-readable form in the electronic edition of the *Astrophysical Journal*.

[a] Includes the blended *R*(3) line.

[b] Includes the blended *R*(4) line.

[c] Includes the blended *R*(5) line.

[d] Includes the blended *Q*(4) line.

[e] Blended with the stronger λ4814.53 line of Fe II.

[f] Includes the weaker λ5020.23 line of Fe II.

[g] The average of the widths of the *R*(11), *R*(10), *R*(9), *R*(8), *R*(7), and *P*(4) lines.

[h] In absorption.

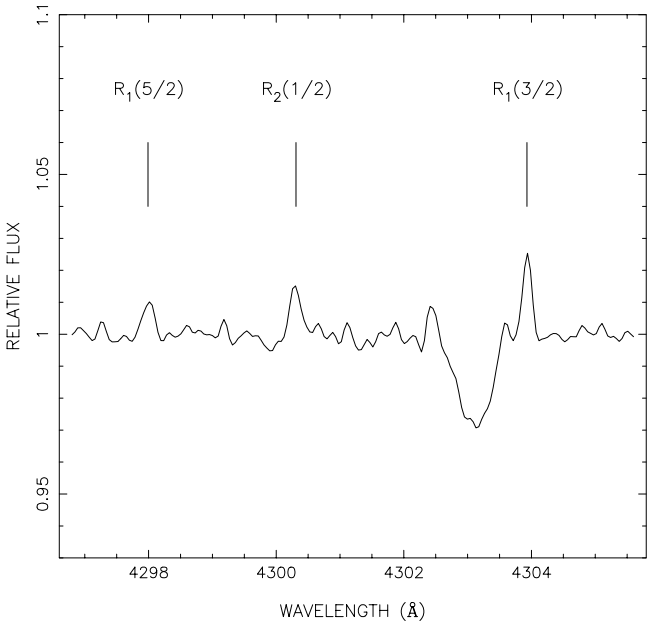

FIG. 2.—The spectrum of HD 44179 near 4300 Å. The positions of the three lines of CH expected to be strongest are shown. The wavelength scale is that in the rest frame of the emitting gas. A weak stellar absorption line of Fe II is also present near 4303.1 Å.

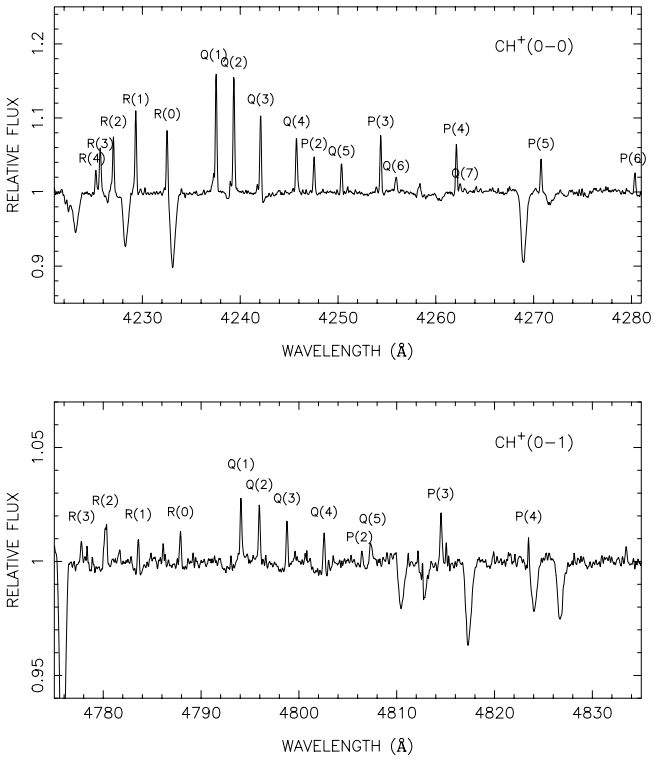

FIG. 3.—*Top*: The spectrum of HD 44179 in the region of the CH^+ A–X (0–0) band. The unlabeled, weak emission line is Fe I λ4258.33 (Table 2). Several stellar absorption lines are present. *Bottom*: The CH^+ (0–1) band, plotted to an expanded vertical scale. The lines of the (0–0) band are stronger than the corresponding lines of the (0–1) band by a factor of roughly 7, which is the ratio of the respective products of the Franck-Condon factor and ν^3.

inferred for the CH^+ molecules seen toward HD 44179 (Bakker et al. 1997). If excited by absorption in the A–X electronic transition, the high-J emission lines in the (0–0) band demonstrate in particular that the ground-state rotational levels of CH^+ are populated with (indirectly) observable abundances up to at least $J = 6$. This is in contrast to the CH emission, indicating that CH^+ and CH may largely exist in different regions of the medium. Since CH^+ has a large dipole moment predicted by ab initio theory to be near 1.7 D (Ornellas & Machado 1986; Follmeg et al. 1987; Sun & Freed 1988), the Einstein coefficient for the $J = 6 \rightarrow 5$ rotational transition is $A \approx 2\ s^{-1}$. In a steady state, this relatively fast rate would require a critical total density on the order of $10^9\ cm^{-3}$. Despite the proximity of HD 44179 to the emitting gas, we assume that radiative pumping of the excited rotational levels in the ground state via A–X (and other) electronic transitions is negligible, compared to collisional excitation of those levels. Collisional thermalization of CH^+ may not proceed effectively, however, since CH^+ molecules are destroyed by both H_2 and H. It is more likely that we are observing freshly produced CH^+ from hydrogen abstraction reactions between C^+ and vibrationally excited H_2^*, $C^+ + H_2^* \leftrightarrow CH^+ + H$, during the short time before CH^+ is destroyed by H_2 (Lambert & Danks 1986; Jura et al. 1997). Low-velocity shocks could also play a significant role (Cernicharo et al. 1997). A fuller analysis is planned for a separate paper.

The rotational levels of the CN ground state are similarly seen to be populated up to $J \approx 14$. With a theoretical dipole moment of 1.361 D (Langhoff & Bauschlicher 1989), the spontaneous emission rate for $J = 14 \rightarrow 13$ is calculated to be $A = 0.085\ s^{-1}$, corresponding to a critical density on the order of $10^8\ cm^{-3}$. (Note that the collision cross section of CN is less than the Langevin cross section of CH^+.) This indicates that the CN is in a region of the medium that shows high density. For comparison, the intensity ratio of two of the [S II] lines, λ6716 and λ6730, yields an independent estimate of the electron density in the [S II]-emitting gas. The observed

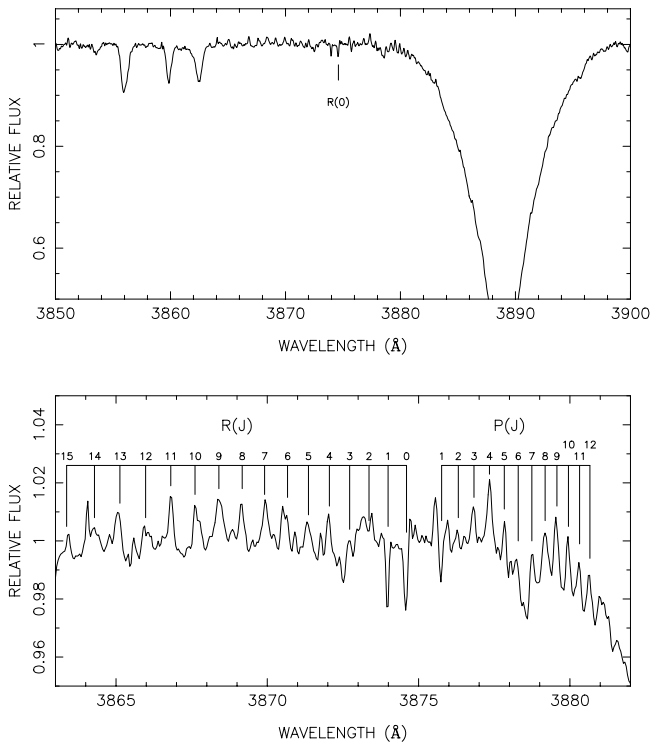

FIG. 4.—The spectrum of HD 44179 in the region near the B–X (0–0) band of CN. The top panel presents an overview; the Balmer Hζ line near 3889.05 Å is evident. The bottom panel provides an expanded view.

intensity ratio found from Table 2, about 0.43, agrees with the corresponding ratio of the products $g_{up}A$, within the uncertainties in both quantities. (The values of the transition probability adopted in Table 2 for these two lines are those of Osterbrock 1989.) In this high-density limit, the inferred electron density is $n_e \gtrsim 10^4$ cm^{-3} (Osterbrock 1989), a value apparently consistent with the total density deduced from the CN emission. The contrasting shapes of the respective line profiles suggest that the CN molecules and the S II ions may occupy largely different spatial regions, however.

The $R(0)$, $R(1)$, and $P(1)$ lines of CN are seen in absorption at effectively the same radial velocity as the many emission lines in Tables 1 and 2; weaker absorption at $J > 1$ may be masked by the corresponding emission components. In marked contrast to the obviously broader emission lines, the three absorption lines are entirely unresolved at our resolution of 8 km s^{-1}. These lines are widely detected as interstellar absorption lines, although they are almost always weaker, and usually much weaker, than their Na I and Ca II counterparts formed in the same cloud. In the spectrum of HD 44179, no very narrow absorption lines of Na I, Ca II, CH, or CH^+ corresponding to the CN absorption are evident. The broader emission line and the blended, still broader stellar absorption line that are also present for each of the two atomic transitions could conceal weak interstellar absorption that arises in a foreground cloud at a similar velocity. In addition, the interstellar CN lines are sometimes stronger than their CH and CH^+ counterparts. Thus, an interstellar origin for the CN absorption cannot be excluded, although we are aware of no other cloud that has been detected in the optical region by means of its CN absorption alone, when suitable observations of the other lines are also available. It seems more likely that, like the many emission lines, the selective absorption by CN arises within the complex envelope of HD 44179.

A small difference in radial velocity may exist between the lines of CH^+ and Fe I, although this possible offset is too small to be measured reliably between any individual pair of lines in our spectra. The average velocity derived from 48 lines of CH^+ is more negative by about 1.3 km s^{-1} than that deduced from 23 Fe I lines, however, and this difference exceeds the combined errors in the mean by a factor of 4.6. The significance of the possible offset is uncertain because of the difference between the line shapes shown by the two species; the Fe I profiles are double-peaked, while the CH^+ lines appear single-peaked at our resolution. Spectra of higher resolution may be able to illuminate this question more conclusively.

3.3. *The Nebular Distance*

The foreground interstellar reddening of HD 44179 is very poorly known and cannot yet provide a useful indirect estimate of the distance to the Red Rectangle. If the star is located at a distance of 700 pc (Men'shchikov et al. 2002), the observed absence of obvious, very narrow interstellar absorption lines of Na I and Ca II (Fig. 2) is noteworthy, however, even though the correlation between stellar distance, in particular, and the strengths of interstellar lines is extremely loose (Hobbs 1974).

The diffuse interstellar band λ5780, and probably the λ6613 band as well, are detected in absorption in our spectra at velocities consistent with those of the atomic and molecular emission lines. The equivalent widths of these two diffuse interstellar absorption bands (DIBs) are about 14 and 7.5 mÅ, respectively, when the former is measured according to the prescription of Thorburn et al. (2003). The DIBs may arise in either the Red Rectangle Nebula or a diffuse interstellar cloud in the foreground, or both. Previous, unsuccessful attempts to identify DIBs formed within other, somewhat similar circumstellar envelopes may provide little relevant information here, because those spectra apparently provided insufficient sensitivity to reveal DIBs as weak as these seen in our spectra (Kendall et al. 2002; Zacs et al. 2003). We note that the good empirical correlation between $W_\lambda(\lambda 5780)$ and the column density N(H I) (Herbig 1993) gives an upper limit $N(\mathrm{H\ I}) \leq 1.0 \times 10^{20}$ cm^{-2} for a hypothetical foreground cloud; the equality obtains only if the DIBs are assumed to arise entirely within the cloud. In this limit, the corresponding interstellar lines of Na I and perhaps Ca II are statistically likely, but not certain, to be detectable in spectra such as ours (Welty et al. 1994, 1996), in contrast to the observed result. Thus, the location in which the DIBs observed in the spectra of HD 44179 have formed is undetermined at present.

At $l = 219\overset{\circ}{.}0$ and $b = -11\overset{\circ}{.}7$, the star is separated on the sky from each of κ Ori and β CMa by approximately 8°. Both of these stars lie closer than 400 pc and at higher Galactic latitudes than HD 44179. Nevertheless, the spectrum of κ Ori shows relatively strong absorption by Na I and Ca II; that of β CMa, at a distance of only about 200 pc, does not. The Local Bubble of very hot interstellar gas, in which the Sun is immersed and in which Na and Ca are highly ionized, is known to extend to a uniquely large distance of up to 500 pc in the general direction of β CMa (Frisch & York 1983; Gry et al. 1985). This may account for the lack of interstellar absorption by Na I and Ca II toward HD 44179 as well; alternatively, a smaller distance to the Red Rectangle of perhaps 330 pc may provide the correct explanation (Cohen et al. 1975). Some of the difficulties posed in turn by this smaller estimate have been reviewed by Men'shchikov et al. (2002). A high-resolution study of interstellar line strengths toward both HD 44179 and a denser grid of comparison stars, specifically chosen to better bracket the star spatially, could provide an improved distance estimate in the future.

4. SUMMARY

We have recorded the spectrum of HD 44179 between 3800 and 10000 Å at a velocity resolution of 8 km s^{-1} and at a maximum S/N of 850 near 6800 Å. A total of 133 emission lines of H I, C I, N II, O I, Na I, Mg I, S II, K I, Ca II, Fe I, Fe II, Rb I, Ba II, CH, CH^+, or CN were measured and identified in the spectrum, along with one unidentified atomic emission line and three absorption lines of CN. On five of the seven nights for which we have data, the heliocentric radial velocity of the relatively strong K I and the [O I] lines was invariant at 19.5 ± 0.4 km s^{-1}, while these lines were blueshifted by about 2 km s^{-1} on the remaining two nights. CO emission in a similar velocity range is observed in the millimeter wavelength range. From extensive temporal monitoring of that emission at velocity resolutions as precise as 0.2 km s^{-1}, Bujarrabal et al. (2003) inferred that the CO-emitting gas lies in an extended, orbiting disk.

The emission, and probably the absorption as well, apparently originate primarily within or near the small, dusty torus that optically obscures HD 44179 and that lies near the center of a much larger envelope of stellar ejecta. A compact H II region and associated, dense neutral gas may produce most of the observed line spectrum, and some of the ground-level lines may arise from resonant scattering of light from the central star. On the basis of their shapes and widths, the line profiles of the various elements can be classified into three groups: narrow, broad, and double-peaked. The lines of C I, K I, Ca II, Fe II, CH,

CH^+, and CN show intrinsic widths FWHM ≤ 15 km s^{-1} and constitute the narrow-lined group. The CN rotational populations imply that at least some of these species exist primarily in neutral gas with a density $n(\mathrm{H}) \gtrsim 10^8$ cm^{-3}. The lines of H I, N II, O I, and S II are much broader and are probably produced in an H II region. The generally weak lines of Mg I, Fe I, Rb I, and Ba II, and of the unidentified atom or ion, are double-peaked. They consist approximately of two components of equal intensity and width, about 12 km s^{-1}, which are separated by 14 km s^{-1}. The spatial location(s) of the gas that produces these lines is unclear, although the width inferred for each of the resolved components agrees with those of the first, narrow-lined group.

Several other results are of special interest:

1. To the best of our knowledge, this is the first case in which Rb I and Ba II emission have been detected from gas in a circumstellar envelope. In view of the accretion process implied by the very peculiar surface abundances of HD 44179, the detection of Ba II in the circumstellar gas lends support to the hypothesis of Waelkens et al. (1996) that the star will evolve into a barium star. No stellar Ba lines are evident in our spectra.

2. Rapid spontaneous emission from excited rotational levels of CH^+ that are populated up to $J = 6$ in the ground electronic state would require densities $n(\mathrm{H}) \geq 10^8$ cm^{-3} in a steady state, presumably in largely neutral gas. Because CH^+ is rapidly destroyed by H_2 and H, the observed spectral lines are likely to be freshly produced by a reaction such as $C^+ + H_2^* \leftrightarrow CH^+ + H$, during the short time before the CH^+ is destroyed.

3. In view of the absence of corresponding interstellar absorption by Na I and Ca II, the three absorption lines of CN are likely to originate in the same gas as some of the emission lines, rather than in a foreground interstellar cloud. The absence in our spectra of narrow interstellar Na I and Ca II absorption lines at any velocity favors weakly a distance to the Red Rectangle that is significantly smaller than 700 pc.

A comprehensive model of the complex Red Rectangle Nebula must include such vital features as those identified by Glinski et al. (1997), Men'shchikov et al. (2002), Bujarrabal et al. (2003), and Cohen et al. (2004), but must eventually add more detail to them. Future papers in this series are planned both to address the molecular chemistry briefly indicated here and to present our nebular spectra that have not been considered here.

We thank the referee for valuable and constructive comments on the initial version of this paper. T. O. acknowledges financial support of this work by the National Science Foundation through grant PHY-0099442 to the University of Chicago. D. G. Y. acknowledges further support of this work by the National Aeronautics and Space Administration, through a subcontract with the University of Chicago that is derived from contract NAS5-32985 with Johns Hopkins University.

REFERENCES

Bakker, E. J., van Dishoeck, E. F., Waters, L. B. F. M., & Schoenmaker, T. 1997, A&A, 323, 469
Baldwin, J. A., Verner, E. M., Verner, D. A., Ferland, G. J., Martin, P. G., Korista, K. T., & Rubin, R. H. 2000, ApJS, 129, 229
Balm, S. P., & Jura, M. 1992, A&A, 261, L25
Bauschlicher, C. W., Langhoff, S. R., & Taylor, P. R. 1988, ApJ, 332, 531
Bond, H. E., Fulton, L. K., Schaefer, K. G., Ciardullo, R., & Sipior, M. 1997, in IAU Symp. 180, Planetary Nebulae, ed. H. J. Habing & H. J. G. L. M. Lamers (Dordrecht: Kluwer), 211
Bujarrabal, V., Neri, R., Alcolea, J., & Kahane, C. 2003, A&A, 409, 573
Carrington, A., & Ramsay, D. A. 1982, Phys. Scr., 25, 272
Cernicharo, J. 2004, ApJ, 608, L41
Cernicharo, J., Liu, X.-W., Gonzalez-Alfonso, E., Cox, P., Barlow, M. J., Lim, T., & Swinyard, B. M. 1997, ApJ, 483, L65
Cohen, M., Van Winckel, H., Bond, H. E., & Gull, T. R. 2004, AJ, 127, 2362
Cohen, M., et al. 1975, ApJ, 196, 179
Dinerstein, H. L., Sneden, C., & Uglum, J. 1995, ApJ, 447, 262
Follmeg, B., Rosmus, P., & Werner, H.-J. 1987, Chem. Phys. Lett., 136, 562
Frisch, P. C., & York, D. G. 1983, ApJ, 271, L59
Glinski, R. J., Lauroesch, J. T., Reese, M. D., & Sitko, M. L. 1997, ApJ, 490, 826
Gry, C., York, D. G., & Vidal-Madjar, A. 1985, ApJ, 296, 593
Hall, D. I., Miles, J. R., Sarre, P. J., & Fossey, S. J. 1992, Nature, 358, 629
Herbig, G. H. 1993, ApJ, 407, 142
Hobbs, L. M. 1974, ApJ, 191, 381
Jura, M., Turner, J., & Balm, S. P. 1997, ApJ, 474, 741
Kendall, T. R., Mauron, N., McCombie, J., & Sarre, P. J. 2002, A&A, 387, 624
Lambert, D. L., & Danks, A. C. 1986, ApJ, 303, 401
Langhoff, S. R., & Bauschlicher, C. W. 1989, ApJ, 340, 620
Larsson, M., & Siegbahn, P. E. M. 1983, Chem. Phys., 76, 175
Luque, J., & Crosley, D. R. 1996, J. Chem. Phys., 104, 2146
Men'shchikov, A. B., Schertl, D., Tuthill, P. G., Weigelt, G., & Yungelson, L. R. 2002, A&A, 393, 867
Oka, T., Thorburn, J. A., McCall, B. J., Friedman, S. D., Hobbs, L. M., Sonnentrucker, P., Welty, D. E., & York, D. G. 2003, ApJ, 582, 823
Ornellas, F. R., & Machado, F. B. C. 1986, J. Chem. Phys., 84, 1296
Osterbrock, D. E. 1989, Astrophysics of Gaseous Nebulae and Active Galactic Nuclei (Mill Valley: University Science Books)
Pequignot, D., & Baluteau, J.-P. 1994, A&A, 283, 593
Prasad, C. V. V., Bernath, P. F., Frum, C., & Engleman, R. 1992, J. Mol. Spectrosc., 151, 459
Roddier, F., Roddier, C., Graves, J. E., & Northcott, M. J. 1995, ApJ, 443, 249
Scarrott, S. M., Watkin, S., Miles, J. R., & Sarre, P. J. 1992, MNRAS, 255, 11P
Schmidt, G. D., Cohen, M., & Margon, B. 1980, ApJ, 239, L133
Schmidt, G. D., & Witt, A. N. 1991, ApJ, 383, 698
Sharpee, B., Williams, R., Baldwin, J. A., & van Hoof, P. A. M. 2003, ApJS, 149, 157
Smith, V. V., & Lambert, D. L. 1987, MNRAS, 226, 563
Sterling, N. C., & Dinerstein, H. L. 2003, Rev. Mex. AA, 18, 133
Sun, H., & Freed, K. F. 1988, J. Chem. Phys., 88, 2659
Thorburn, J. A., et al. 2003, ApJ, 584, 339
Van Winckel, H., Cohen, M., & Gull, T. R. 2002, A&A, 390, 147
Van Winckel, H., Waelkens, C., & Waters, L. B. F. M. 1995, A&A, 293, L25
Vijh, U. P., Witt, A. N., & Gordon, K. D. 2004, ApJ, 606, L65
Waelkens, C., Van Winckel, H., Bogaert, E., & Trams, N. R. 1991, A&A, 251, 495
Waelkens, C., Van Winckel, H., Trams, N. R., & Waters, L. B. F. M. 1992, A&A, 256, L15
Waelkens, C., Van Winckel, H., Waters, L. B. F. M., & Bakker, E. J. 1996, A&A, 314, L17
Wang, S., et al. 2003, Proc. SPIE, 4841, 1145
Warren-Smith, R. F., Scarrott, S. M., & Murdin, P. 1981, Nature, 292, 317
Welty, D. E., Hobbs, L. M., & Kulkarni, V. P. 1994, ApJ, 436, 152
Welty, D. E., Morton, D. C., & Hobbs, L. M. 1996, ApJS, 106, 533
Zachwieja, M. 1995, J. Mol. Spectrosc., 170, 285
Zacs, L., Spelmanis, R., Musaev, F. A., & Galazutdinov, G. A. 2003, MNRAS, 339, 460